

Article

Copper-Containing Agates of the Avacha Bay (Eastern Kamchatka, Russia)

Galina Palyanova ^{1,2,*} , Evgeny Sidorov ³, Andrey Borovikov ² and Yurii Seryotkin ^{1,2} 

¹ Sobolev Institute of Geology and Mineralogy, Siberian Branch of Russian Academy of Sciences, Akademika Koptyuga pr. 3, 630090 Novosibirsk, Russia; yuvs@igm.nsc.ru

² Department of Geology and Geophysics, Novosibirsk State University, Pirogova str. 2, 630090 Novosibirsk, Russia; borovikov.57@mail.ru

³ Institute of Volcanology and Seismology, Far East Branch of Russian Academy of Sciences, Piipa Blvd. 9, 683006 Petropavlovsk-Kamchatsky, Russia; mineral@kscnet.ru

* Correspondence: palyan@igm.nsc.ru

Received: 22 October 2020; Accepted: 8 December 2020; Published: 14 December 2020



Abstract: The copper-containing agates of the Avacha Bay (Eastern Kamchatka, Russia) have been investigated in this study. Optical microscopy, scanning electron microscopy, electron microprobe analysis, X-ray powder diffraction, Raman spectroscopy, and fluid inclusions were used to investigate the samples. It was found that copper mineralization in agates is represented by native copper, copper sulphides (chalcocite, djurleite, digenite, anilite, yarrowite, rarely chalcopyrite) and cuprite. In addition to copper minerals, sphalerite and native silver were also found in the agates. Native copper is localized in a siliceous matrix in the form of inclusions usually less than 100 microns in size—rarely up to 1 mm—forming dendrites and crystals of a cubic system. Copper sulphides are found in the interstices of chalcedony often cementing the marginal parts of spherule aggregates of silica. In addition, they fill the micro veins, which occupy a cross-cutting position with respect to the concentric bands of chalcedony. The idiomorphic appearance of native copper crystals and clear boundaries with the silica matrix suggest their simultaneous crystallization. Copper sulphides, cuprite, and barite micro veins indicate a later deposition. Raman spectroscopy and X-ray powder diffraction results demonstrated that the Avacha Bay agates contained cristobalite in addition to quartz and moganite. The fluid inclusions study shows that the crystalline quartz in the center of the nodule in agates was formed with the participation of solutions containing a very low salt concentration (<0.3 wt.% NaCl equivalent) at the temperature range 110–50 °C and below. The main salt components were CaCl₂ and NaCl, with a probable admixture of MgCl₂. The copper mineralization in the agates of the Avacha Bay established in the volcanic strata can serve as a direct sign of their metallogenic specialization.

Keywords: agate; Avacha Bay; Kamchatka; Russia; copper; SEM; EPMA; XRD; RS; inclusions; genesis

1. Introduction

The mineralogy of agate nodules in basalts has been studied and summarized in many papers [1–19]. Agate is a banded chalcedony, which can be intergrown or intercalated with other silica phases (macro-crystalline quartz, quartzine, opal-A, opal-CT, cristobalite, and moganite) [8]. Some common secondary minerals can be found in agate. Oxides of iron add color, but calcite would be regarded as an impurity. Celadonite is often found as an outer coating but can be found in the agate from basic igneous hosts. Nevertheless, copper and copper minerals in agates are rare. The copper-included agates were originally collected in 1952 [20], despite this, the number of papers on them is relatively small [21].

Agates containing native copper and (or) copper sulphides have been identified in some deposits [18–28]. Native copper, cuprite, and zincite are found in the Ayaguz agate deposit (East Kazakhstan) [18]. Here, native copper plates and grains are located in the second cristobalite-chalcedony zone, following a thin first outer zone of an oval-shaped chalcedony. Native copper and copper minerals are often an intergrowth with cristobalite spheroids and cuprite. Additionally, Radko [22] notes the presence of a fine impregnation of native copper and copper oxides in agates of the Norilsk region (Russia). This dispersion of micro grains of copper gives them a reddish color.

Native copper was noted locally, but in considerable concentrations in an inner agate laminae of “bituminous” agates from Nowy Kościół (Lower Silesia, Poland) [23]. Copper-banded agates, in which native copper sometimes fills up to 80% of a nodule’s volume, are known from the Wolverine Mine, Wolverine, Houghton County, Michigan (USA) [19,21]. These unusual agates, which range in size from 1 to 4 cm across, occur in a basaltic lava flow that is approximately 1100 Ma. This makes them, along with the regular Lake Superior agates, the oldest agates on the American continent [10]. The Kearsarge copper-bearing amygdaloidal lode in Houghton County, Michigan (USA) formed commercial ore bodies [21]. Nezafati et al. [24] considered the Darhand copper occurrence in Central Iran as an example of Michigan-type native copper deposits.

The genesis of agates with native copper and copper sulphides has been discussed in few papers [18,19,21,24–28]. Agates with native copper were found in paleobasalts from Rudno near Krzeszowice in Lower Silesia (Poland) [25]. The native copper inclusions are irregular with jagged edges and ranged in size from 0.01 to 2 mm. The analyses of sections also showed cuprite, apart from native copper. Cuprite occurs at the contact of native copper and chalcedony or even replaces the former, creating separate pockets. The relation of copper mineralization to other minerals of the agate paragenesis suggests its secondary origin and formation in the zone of oxidation.

Copper sulphides without native copper are found in agates from Sidi Rahal and Kerrouchen (Khénifra Province, Meknés-Tafilalet Region), in the Atlas mountains of Morocco [26,27]. Moroccan agates occur within Triassic basaltoids as lens-shaped specimens in sizes up to 25–30 cm. Tiny single crystals of copper sulphides (unknown composition) have been found in the central part of agate nodules from Sidi Rahal and were accompanied by idiomorphic quartz [26]. Copper sulphides, calcite, and an organic substance were incorporated during post-magmatic, hydrothermal or hypergenic conditions. The aggregates of copper sulphides and titanium oxides (rutile) in agate nodules from Kerrouchen (Khénifra Province, Meknés-Tafilalet Region) in Morocco [27] were most likely deposited during post-magmatic processes. It was also proposed that the origin of solid bitumen in these agates was the result of low temperature hydrothermal or hypergenic processes.

Powolny et al. [28] studied vein agates and moss agates, which were encountered for the first time within spilitized (albite-rich) alkali-basalts from the upper parts of the Borówno quarry (Intra-Sudetic Basin, Lower Silesia, Poland). Vein agates consist predominately of length-fast chalcedony evolving into strongly zoned prismatic quartz with numerous solid inclusions such as Fe-Cu sulphides that included chalcocite and chalcopyrite.

Agate-bearing strata have been detected in the vicinity of Petropavlovsk-Kamchatsky, located along the eastern shore of Avacha Bay (Eastern Kamchatka, Russia). Sidorov et al. [29] were the first to report native copper inclusions in agates from the Shlyupochnaya Bay in the Avacha Bay. However, to date, detailed studies of agates with copper have not been made. Taking this into account, the authors in the present paper undertook to carry out detailed researches of the copper containing agates, using a set of various analytical methods: optical microscopy, scanning electron microscopy (SEM), electron microprobe analysis (EPMA), X-ray powder diffraction (XRD), Raman spectroscopy (RS), and fluid inclusions studies.

The prime objective of this study is to examine the copper and other minerals in agates of the Eastern Kamchatka, Russia. Of particular interest was the relationship between copper and the supporting silica minerals. The article provides new information on the mineralogical features of agates

from the coastal outcrops of Shlyupochnaya Bay in the Avacha Bay and substantiates the conditions for the genesis of copper mineralization in agates. The copper content of the Avacha Bay agates is low compared to similar agates from Michigan, USA. Nevertheless, the Avacha Bay agates have sufficient copper and compounds to allow comment on its possible genesis.

2. Geological Setting and Description of Agates

2.1. Geological Setting

Agate-containing strata are found along the eastern coast of Avacha Bay (Figure 1). The most ancient formations developed along this territory are the volcanic-sedimentary deposits of the Nikolskaya strata (K_2nk) [30]. The strata is divided into two substructures: the lower strata is a layer of green clay schist and siliceous schist with weakly metamorphosed sandstone, siltstone and mudstone. The upper substructure is composed of volcanogenic-terrigenous rocks: siliceous rocks, metamorphosed siltstone and sandstone, greenstone altered tuffs, and spherical basalt.

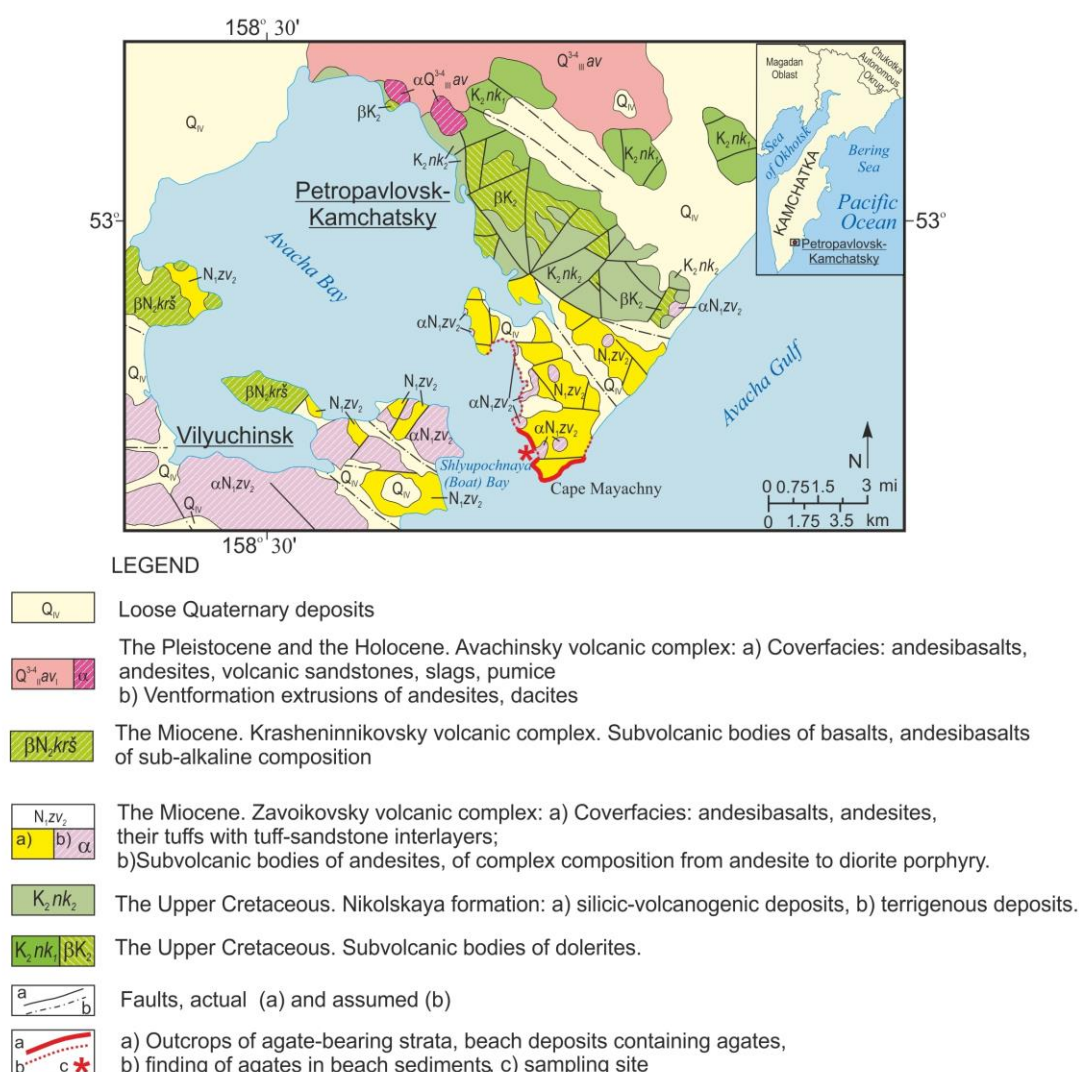


Figure 1. Simplified geological map of the shore of the Avacha Bay with agate occurrences (Q_w), after Sheymovich [30].

The Late Cretaceous age of the Nikolskaya formation was determined from the discovered remains of fauna, spores, and pollen in the northern part of the city area [30,31]. Cretaceous rocks are overlain by tuff of the early phase of the Avacha volcanic complex of Pleistocene-Holocene age (Figure 1).

Agate-bearing effusive-pyroclastic formations in the vicinity of Petropavlovsk-Kamchatsky exposed in the cliffs along the shores of the Avacha Bay and on the ocean coast are united in the Zavoykovsky complex. This complex combines cover and subvolcanic intrusive formations developed in the coastal zone of the Avacha Bay. The cover phase unites lava flows, lavobrecchia, and the tuff of predominantly andesite/basalt composition. Effusive-pyroclastic formations are common in the shore cliffs of the Avacha Bay [31].

Tuffs, mainly agglomerate, rarely psephite, occur as separate layers with a thickness of 10 to 40 m—rarely up to 150 m. Among the lavas, porphyritic rocks prevail andesites and basalts. Subvolcanic formations are represented by stocks, which are dominated by andesite and bodies of complex structure, the composition of which varies from andesite to diorite porphyrite. Morphologically, subvolcanic bodies are often distinguished in the form of separate dome-shaped peaks; in plain view they have an oval shape. The area of their outcrops ranges from 0.5 to 40 km².

The effusive-pyroclastic facies of the volcanic complex contain organogenic remains that indicate the Miocene age of the enclosing sediments. This dating was later confirmed by the K-Ar age determinations of subvolcanic intrusions of andesite composition. Their ages are in the range of 12.5 to 18.4 Ma [30].

Low grade metamorphism of the agate-containing Miocene volcanic rocks is characterized by the zeolite facies and the uneven processing of the rocks. Secondary minerals are dominated by zeolites, hematite, goethite, calcite, and corrensite. Celadonite stains the rock bright green [32].

Agates and chalcedony are detected among the lava flows and breccia of the late phase of the Zavoykovsky complex. The agates are to be found in veins, veinlets, and rounded openings. The latter can be 20 cm in diameter.

At the foot of rocky coastal cliffs are exposures of volcanites with an almond-stone texture. These were formed by contractions and veinlets of agate and chalcedony in the host volcanites (Figure 2a,b). Well-rounded beach agates show that agates are being released from the host rock.



Figure 2. (a) Coastal outcrops of Shlyupochnaya Bay (Avacha Bay, Eastern Kamchatka, Russia) (photo G. Palyanova); (b) agate nodules (1–10 cm) in basalt (photo by D. Bukhanova).

2.2. Description of Agates

The agates from the coastal zone of the Avacha Bay are grey but can show a bluish tint that can reach a sapphire blue color in intensity [29,33]. The agate bands range in size and generally show alternating zones of a bluish color. Moss agates can be found but are less common. One unusual feature of agates and chalcedony from the Zavoykovsky volcanites is the frequent presence of native copper. These copper inclusions can range in size from fractions of 10 µm up to 1 mm. Native copper in these agates shows a variety of forms: filamentary aggregates, thin plates, dendrites, and individual perfectly faceted cubic crystals, octahedra and their twins [29]. Figure 3 shows a fragment of rock with dendrites of native copper in the cubic habit, mainly octahedrons.

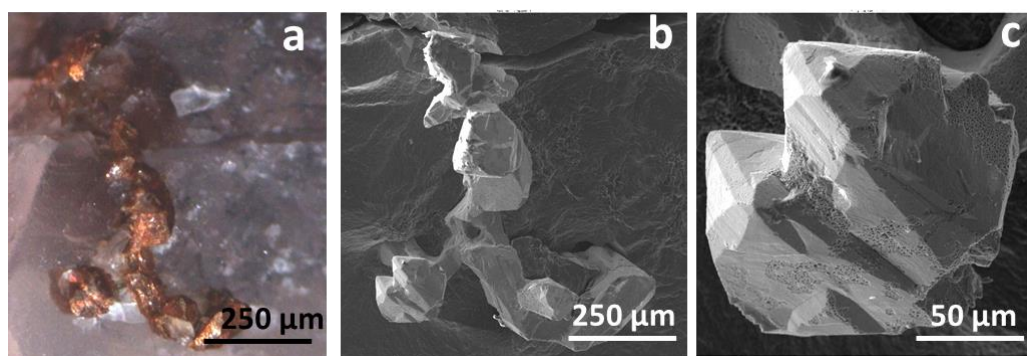


Figure 3. The dendrites of native copper on the surface of a fragment of rock. (a) Photo by G. Palyanova, (b,c) SEM micrographs.

3. Materials and Methods

The research was based on the collection of agates and agate-bearing basalts from the Avacha Bay (Eastern Kamchatka, Russia). Agates were taken from the coastal outcrop and coastal strip of Shlyupochnaya Bay (Figure 2). The agates were examined using optical microscopy, SEM, EPMA, XRD, RS, and a fluid inclusions study. Analytical studies were carried out in the Analytical Centre for Multielemental and Isotope Research SB RAS (Novosibirsk, Russia). Preliminary results of electron microprobe analysis of inclusions in agates were obtained in the Institute of Volcanology and Seismology, Far East Branch of Russian Academy of Sciences (Petropavlovsk-Kamchatsky, Russia).

The four typical samples of agates Nos. 4, 5, 7, 8 shown in Figures 4a–c and 8a were prepared by being polished and cut into thin sections. The thickness of the thin sections was 0.09 mm. Agate No. 8 with macrocrystalline quartz in the center of the nodule (Figure 8a) was selected for the study of fluid inclusions.

Polished and thin sections of all agate samples were examined with an Olympus BX 51 (Olympus NDT, Inc., USA) polarizing microscope with a magnification range from 40× to 400×. The agates have been examined using SEM with EDS and XRD techniques. Chemical analyses of mineral phases were carried out using a MIRA LMU electron scanning microscope (TESCAN, Czech) with an INCA Energy 450p X-Max energy-dispersion spectrometer (Oxford Instruments, UK). The operation conditions were: an accelerating voltage of 20 kV, a probe current of 1 nA and a spectrum recording time of 15 to 20 s.

The XRD experiments were performed using X-ray powder diffractometer ARL X'Tra (Thermo Scientific) (CuK α radiation, 40 kV, 25 mA) equipped with a linear detector. Powder diffraction patterns were collected over the 2 θ angular range of 5 to 60 with a speed rotation of 5° 2 θ and 17 to 30 with a speed rotation of 2° 2 θ . Phase analysis was carried out using the PDF-4 database (The Powder Diffraction File PDF-4p) [34].

Raman spectra of silica phases were recorded using a Ramanor U-1000 spectrometer (Horiba Scientific, Japan), with detector JobinYvon LabRAM HR800 (Jobin Yvon Instruments S.A. Inc., France) and a laser MillenniaPro (Spectra-Physics, USA) with a nominal wavelength of $\lambda = 532$ nm. An upright microscope Olympus BX-51 WI with a 100 magnifying objective was used to direct the laser beam onto the sample and to collect the Raman signal under the following parameters: spectral resolution of 2.09 cm $^{-1}$, exposure time of 10 s, five repetitions and filtration D1. The spectra were calibrated against the emission lines of a standard neon lamp, and the peak positions were accurate to within 0.2 cm $^{-1}$.

Cryo- and thermometry methods were used to determine the temperatures of phase transitions in fluid inclusions in quartz (a THMSG-600 microthermal chamber from “Linkam” with a measurement range of −196/+600 °C). The total concentrations of salts in solutions of fluid inclusions and their belonging to one or another water-salt system were determined using the cryometry method [35–37].

4. Results

4.1. Macro- and Microscopic Observations

The nodule agates were mostly oval (Figure 4a,b, agates No. 5, 4; Figure 8a, agate No. 8) or a deformed oval form (Figure 4c, agate No. 7). The size of agates was up to 10 cm. The colors of these agates range from light blue to ash gray tones, often with a reddish tint. Numerous reddish native copper inclusions are concentrated in the margins of agates and include black or beige rock fragments (basalts and altered basalts) (Figure 4e,f).

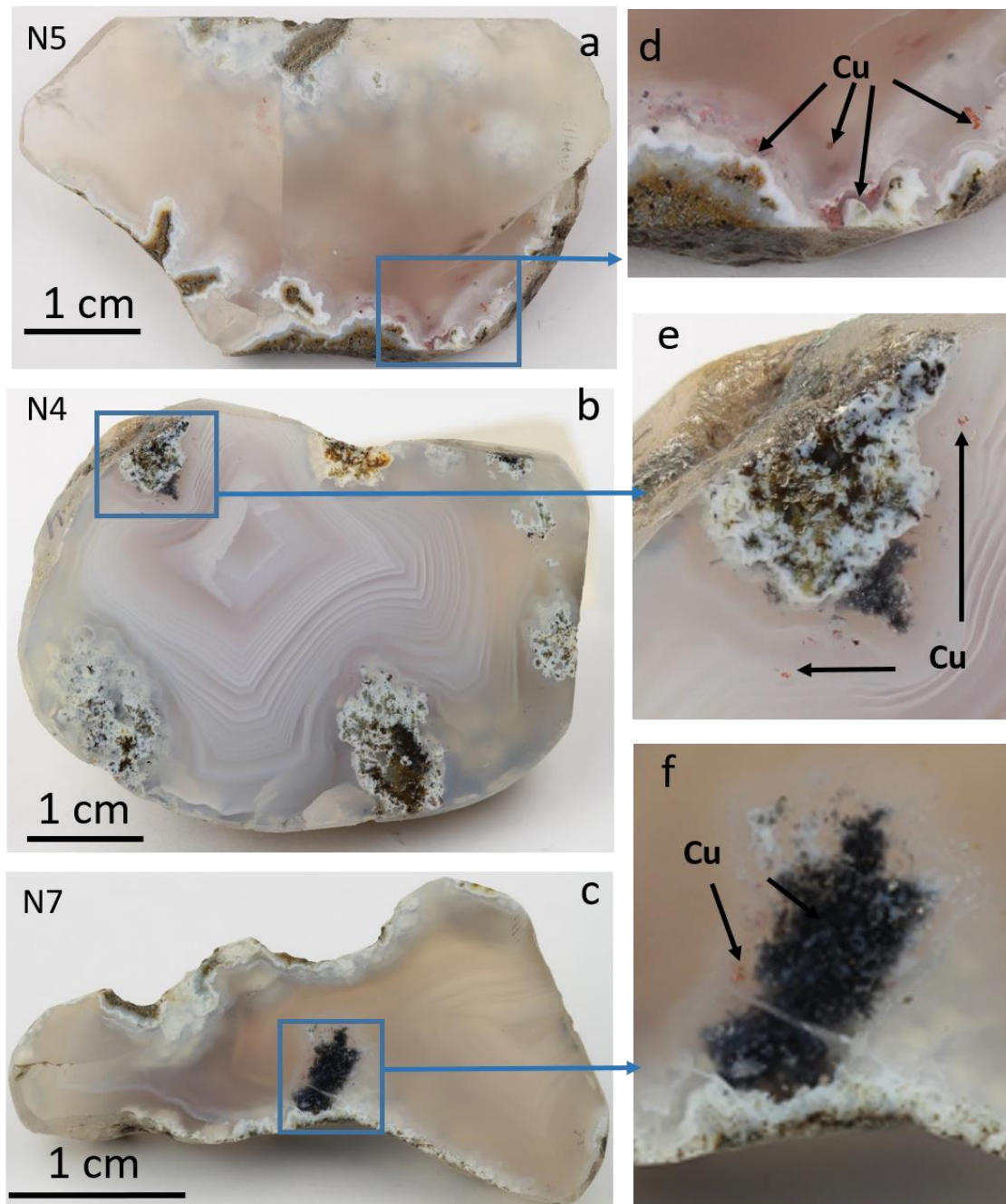


Figure 4. Macrophotographs of studied agates (a–c) and enlarged fragments (d–f) with microinclusions of native copper (red) and other minerals. The Avacha Bay (East Kamchatka, Russia). Polish sections of agates. Photos by A. Vishnevskii.

The tested agate samples differ in morphology. In Figure 4a, the silica matrix of agate No. 5 seems to be almost homogeneous. In this agate, the concentric layers are only in the outer region and absent in the center. Agate No. 4 (Figure 4b,e) belongs to the mono-centric type with elements of “moss agate” on the edge of the nodule. Agate No. 7 (Figure 4c,d) has a more irregular shape and is polycentric, also with fragments of “moss agate” in the marginal parts of the nodule [38]. Agate No. 8 contains the fragments of “moss agate” and crystalline quartz in the center of the nodule (Figure 8a).

From the periphery to the center of the tested agate nodule, the white shell is replaced by alternating layers of different colors and transparency. The outer hardened white shell, characteristic of agates, was fully or partially preserved in the studied agates 5 and 7. It repeats the shape of agate almonds and fragments of host rocks in agates, which act as seeds, around which a white shell is noted.

The microstructure of agates (Nos. 4, 5, 7) is shown in Figures 5–7. For the outer part of agate No. 5 and agates No. 4 and 7, a fibrous and twisted-fibrous texture (wavy fibers) is typical. Microscopically, intergrowth of length-slow and length-fast chalcedony (Figures 5c, 6b and 7d) is clearly visible. The micrographs in transmitted light (crossed polars) of the edge parts of agate, shows the presence of chalcedony spherulites (Figure 9c).

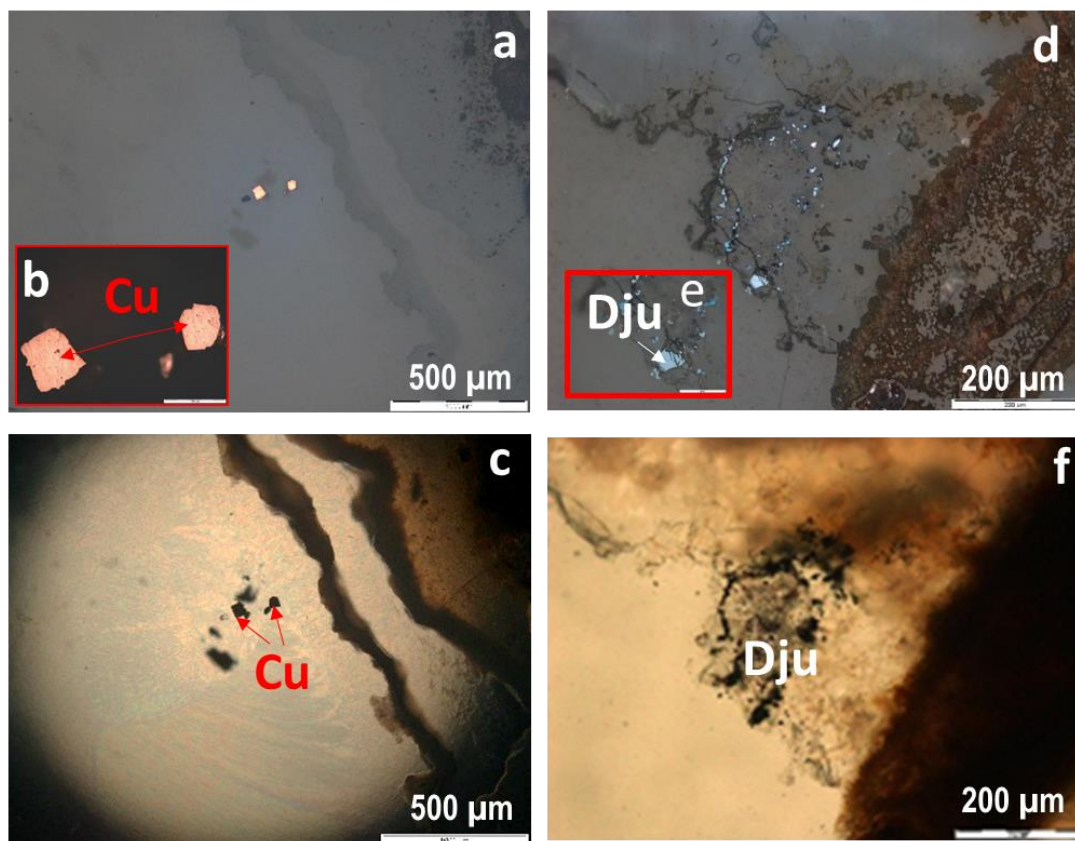


Figure 5. Inclusions of native copper (Cu) (a–c) and djurleite (Dju) (d–f) surrounded by chalcedony in the outer part of agate No. 5 (Figure 4a): (a,b,d,e), in reflected light; (c,f), in transmitted light.

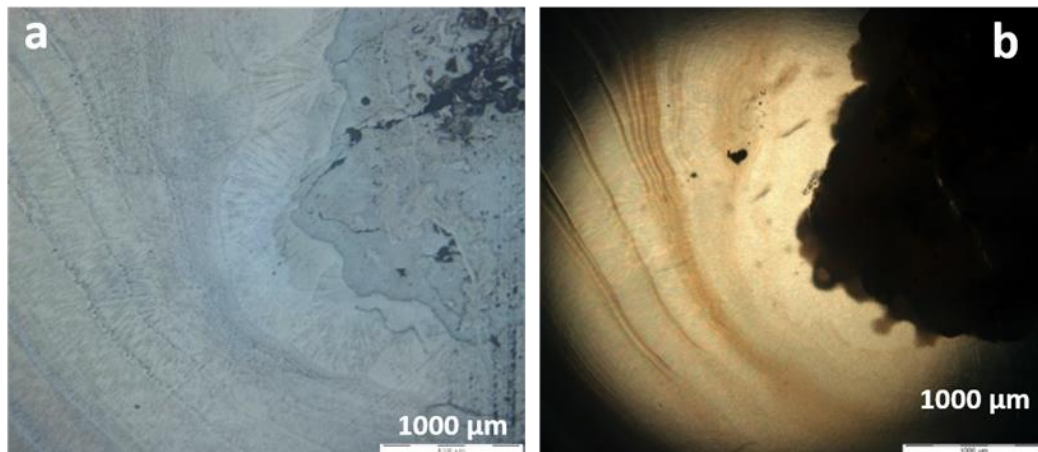


Figure 6. Microstructure of agate No. 4 (Figure 4b) near rock fragments: (a) in reflected light; (b) in transmitted light. A thin section of the agate.

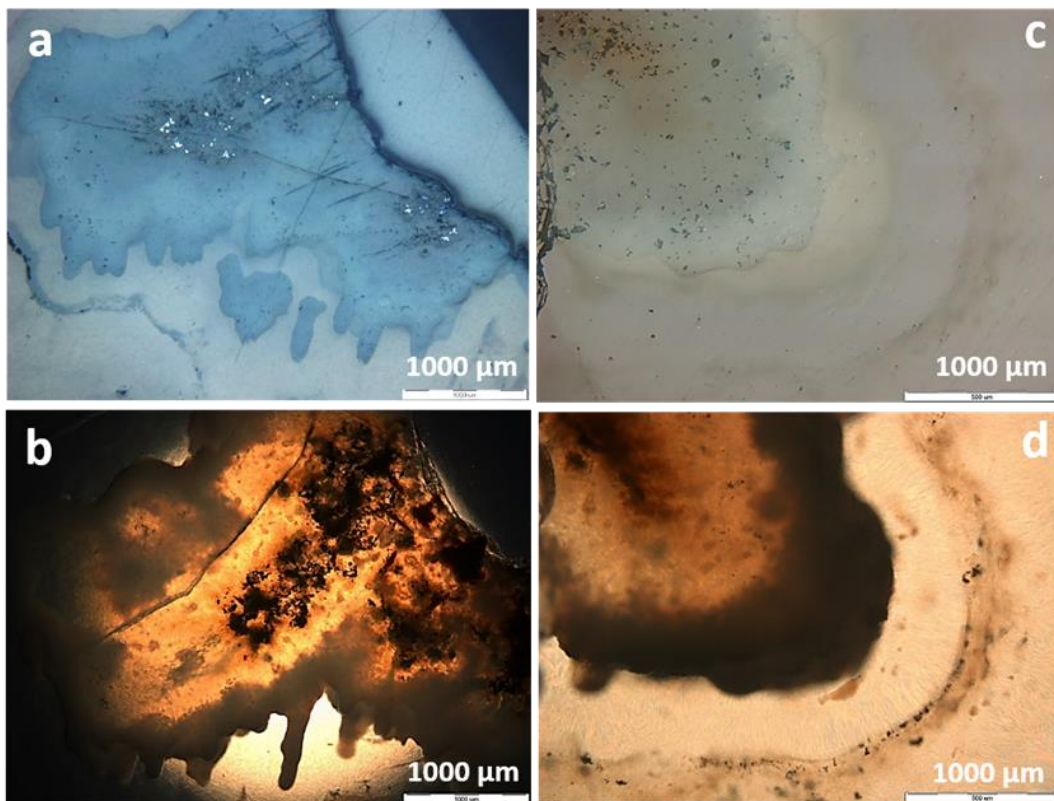


Figure 7. Microstructure of agate No. 7 (Figure 4c) with near inclusions of copper sulphides: (a,c) in reflected light; (b,d) in transmitted light. A thin section of the agate.

The form of the copper minerals is varied. The idiomorphic crystals of a cubic habit indicate the presence of native copper (10–500 µm in size) or their dendrites that are intergrown with silica (Figure 5a, Figures 8a and 9c). A significant part of the copper dendrites is located in the outer marginal zones of the agate nodules near rock fragments (Figure 4d–f). There are clear boundaries of crystals of native copper within a silica matrix.

Copper sulphides form clusters of individual grains in the interstices of chalcedony (Figure 5d,f and Figure 7). The grains range in size from 0.1 mm to 1 micron. Inclusions of copper sulphides are often concentrated in the marginal parts of chalcedony spherulites and are in the form of hypidiomorphic

grains. Native copper is sometimes located in the center of spherulites formed by copper sulphide dendrites and chalcedony (Figures 13 and 14, see Section 4.3).

Native copper, cuprite, chalcocopyrite, sphalerite, and native silver (Figure 8b–f) were determined in agate No. 8 (Figure 8a), with a macrocrystalline quartz in the center of the nodule. The diagnostics of ore minerals were based on their optical properties, established by microscopic examination in reflected light. Later, their compositions were confirmed by EPMA.

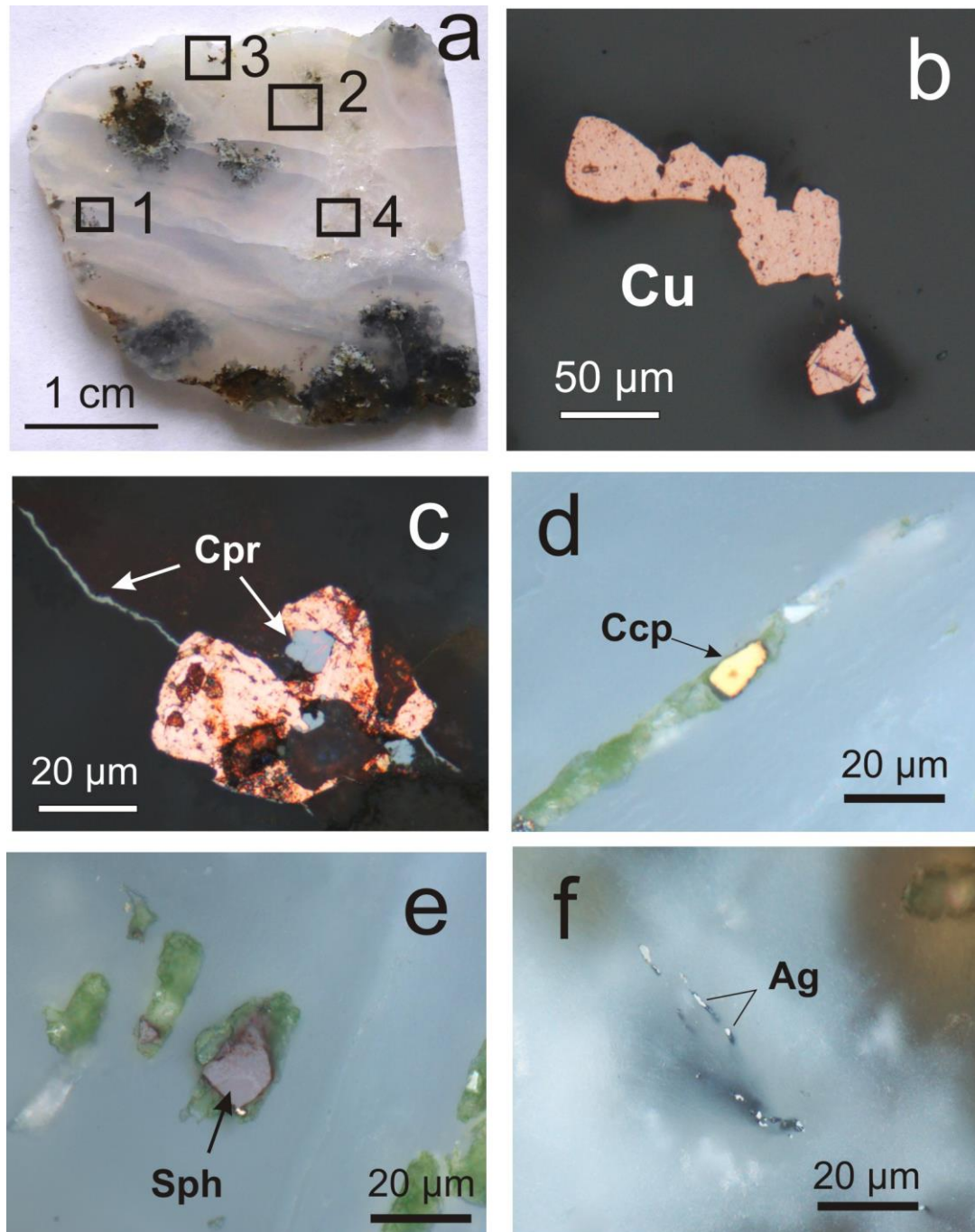


Figure 8. Macrophotograph of the agate No. 8 (a) and ore minerals in it (b–f): (b) dendrites of native copper; (c) cuprite (Cpr) (veins and inclusions) in intergrowth with native copper (Cu) among fine-grained quartz; (d) chalcocopyrite (Ccp) in a cavity in a pseudomorphs of quartz (Figure 9d); (e) sphalerite (Sph); (f) native silver (Ag). (b–f) micrographs in reflected light. Squares 1–4 are RS research areas.

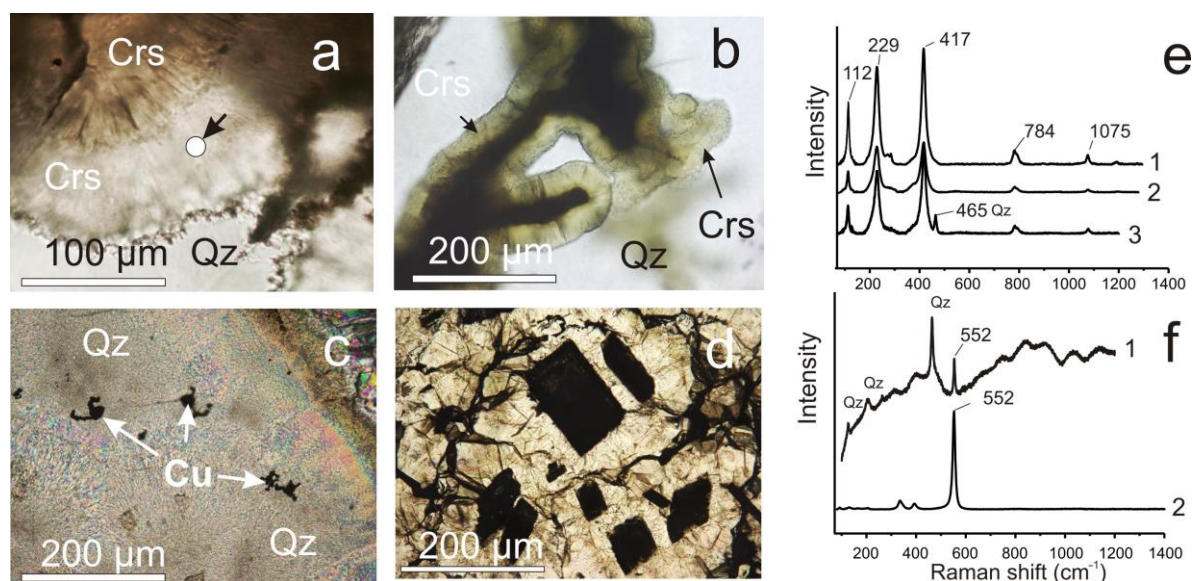


Figure 9. Photographs in the transmitted light of agate No. 8 with native copper: (a) cristobalite, the arrow indicates one of the points of exposure of its Raman spectrum (Figure 9e, spectrum 3); (b) cristobalite among a fine-grained aggregate of spherulite quartz; (c) grains of native copper in quartz at the contacts of intergrown quartz spherulites (crossed polars); (d) voids of leaching among quartz. The voids are partially filled with quartz aggregate. Raman spectra of the agate: (e) spectra of cristobalite (1 and 2) from the RRUFF database [39], respectively, cristobalite spectra X050046 and X050047; the colloform SiO₂ structures spectrum (3) in the point of exposure Figure 9a; (f) spectrum of SiO₂ and cryolite on the surface of the void (1) among quartz and the spectrum of cryolite (2) from the RRUFF database, Cryolite R050287 [39].

4.2. Raman Spectroscopy Results

Raman spectroscopy was used to study agate No. 8 with crystalline quartz in the center of the nodule (Figure 8a) and zonal agate No. 4 (Figure 4b).

Figure 9 shows the varieties of SiO₂ in agate No. 8 (Figure 8a). Cristobalite is present among the fine grained quartz spherulite aggregate (Figure 9a,b). Microinclusions of native copper are located near accrete sintered buds of quartz aggregate (Figure 9c). The coarse quartz of the geode contains quartz pseudomorphs after colloform silica aggregates, which have filled the leaching voids (Figure 9d). They sometimes form complete pseudomorphs. The identification of varieties of SiO₂ were based on their Raman spectrum from the RRUFF database [39] (Figure 9e,f).

The regions of zonal agate No. 4 with different crystallization time and texture were studied. The earliest formations inside the nodule are dark areas with a “moss” texture that is confined to its periphery (Figure 4b,e). These areas are wrapped in alternating concentric layers of transparent and translucent silica, which fills the central portions of the nodule (Figure 10a). According to Raman spectroscopy data [39], the substance of the “moss” formations is represented by an aggregate of cristobalite and fluorophlogopite KMg₃(Si₃Al)O₁₀F₂ (Figure 10a,b).

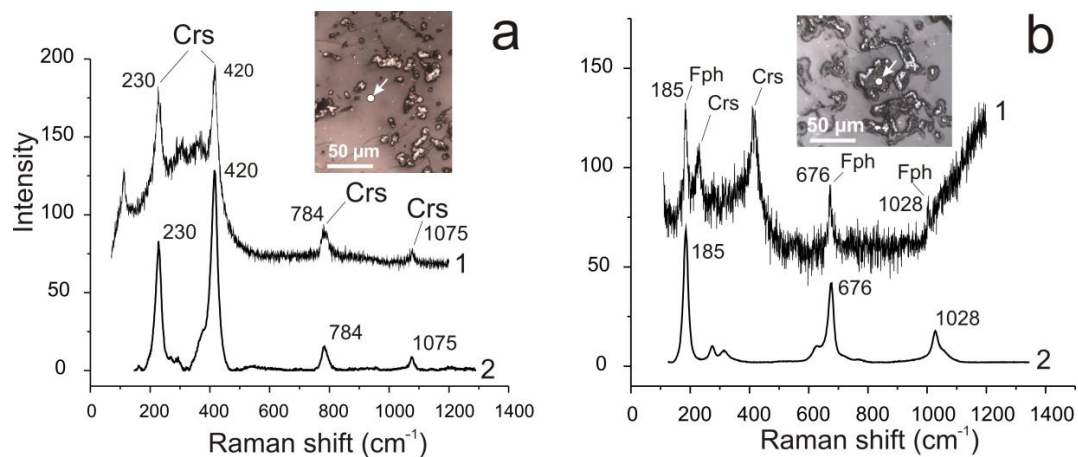


Figure 10. Raman spectra of “moss” aggregates in semitransparent (a) and cristobalite areas (b) in the thin section fragment of agate No. 4 (Figure 4b,e). The exposure sites are taken in reflected light. (a) a spectrum of SiO₂ in a semitransparent area (1) together with an cristobalite spectrum (2) from the RRUFF database the spectrum R060648 [39] (<https://rruff.info/>); (b) the combined spectrum of cristobalite and fluorophlogopite (Fph) (1) in the cristobalite area, compared with the spectrum of fluorophlogopite (2) from the RRUFF database, the spectrum R040075 [39].

The silica that forms the later concentric textures in the center of the nodule is mostly quartz. At the same time, in all the obtained silica spectra of this part of the nodule, the Raman band of moganite is at 503 cm⁻¹, which suggests the presence of this phase in the studied sample. This is also confirmed by similar Raman spectra of numerous agate layers of different transparency near the central part of the agate, where the “moss” formations are absent (Figure 11).

“Moss” white formations in agate No. 4 consist of cristobalite, which is easily identified by the 229 and 418 cm⁻¹ lines, according to Raman standards from the RRUFF database [39]. The α-quartz with admixture of moganite folds up light concentric zones (Figure 11a).

The most intense quartz and moganite bands are shown at 465 and 503 cm⁻¹, respectively (Figure 11). The ratio of the main quartz and moganite bands provides information about the relative abundances of these two silica phases. The value of this ratio is much less than unity, which lies outside the scope of the formula based on the data from Goetze [40] and does not allow quantitative determination of the percentage of content of moganite. However, it can be said that quartz prevails over moganite.

4.3. Scanning Electron Microscopy and Electron Microprobe Analysis Results

The EPMA results of native copper in the agates from the Avacha Bay showed the absence of impurities. Figure 12 shows the distribution of elements over the scanning area from the thin section of agate No. 5 containing the inclusion of a cubic crystal of native copper in a silica matrix. Attention should be paid to the clear boundaries and contacts of native copper with quartz.

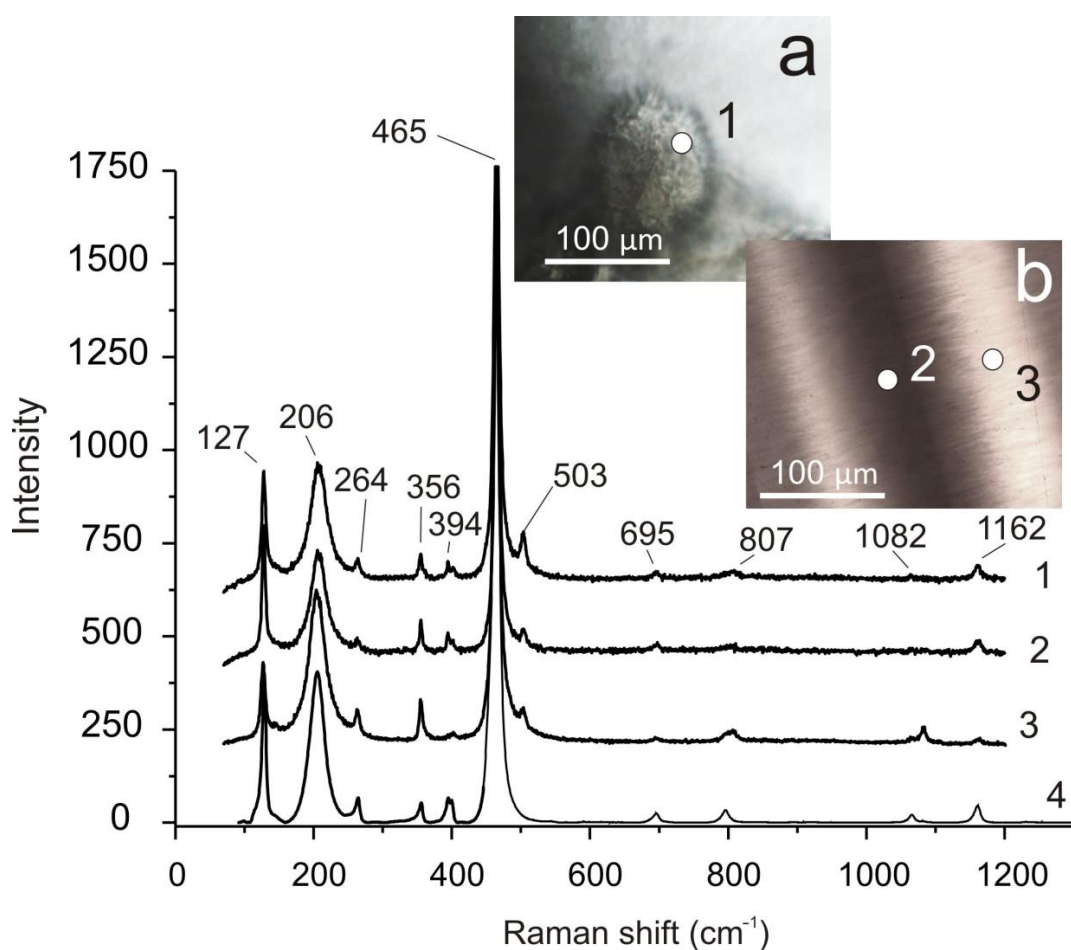


Figure 11. Raman spectra of agate No. 4 (Figure 4b,e) have been taken at various exposure points (1–3) shown in the micrographs (a,b) that were taken in transmitted light. Spectrum 1 is from a semitransparent globule (a) located on the periphery of “moss” aggregates. The micrograph b and spectras 2 and 3 are the respective translucent and transparent layers at the center of the nodule. The most intense quartz and moganite bands are shown at 465 and 503 cm^{-1} , respectively. All other bands are quartz signals. Spectrum 4 is quartz (X080016) from the RRUFF database [39].

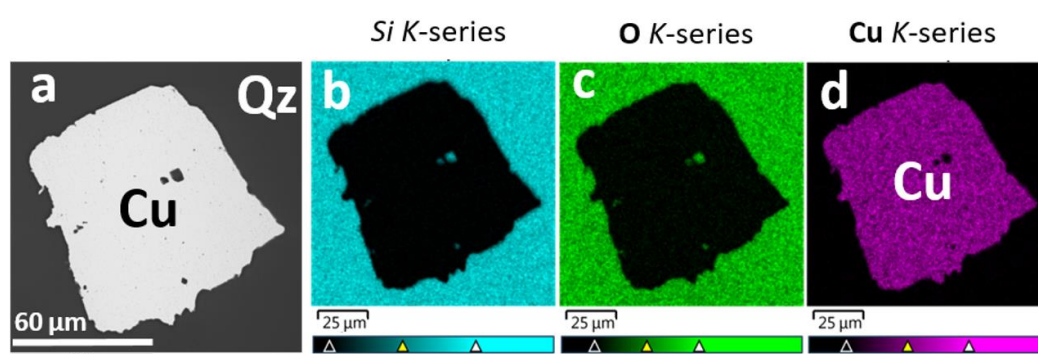


Figure 12. Native copper in a silica matrix: (a) SE micrograph, (b–d) distribution of elements over the scanning area from the thin section of agate No. 5 (Figure 4a,d).

The inclusions of copper sulphides—djurleite ($\text{Cu}_{1.96}\text{S}$), anilite ($\text{Cu}_{1.75}\text{S}$), and yarrowite ($\text{Cu}_{1.1}\text{S}$)—were located in the interstices of a fine-grained spherulitic aggregate of quartz (Figure 13a,b). Djurleite and barite (BaSO_4) filled the micro veins (Figure 13c,d).

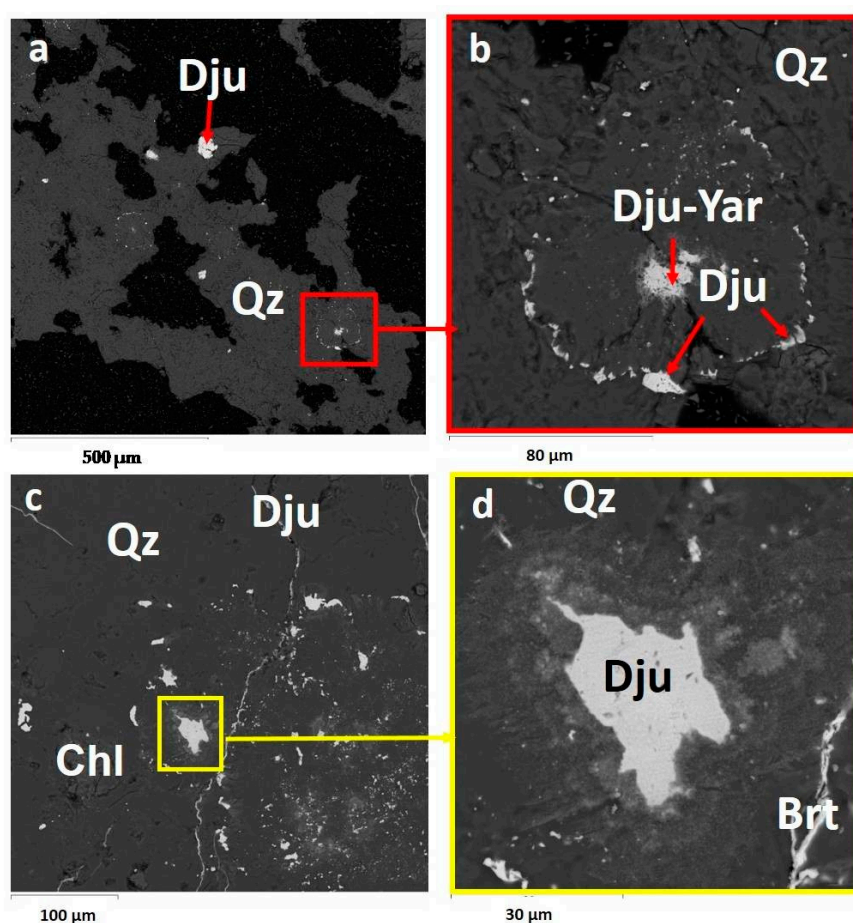


Figure 13. SE micrographs of fragments of agate No. 5 (Figure 4d) with inclusions of copper sulphides: (a,b) djurleite-anilite-yarrowite (Dju-Yar) were present in the interstices of fine-grained spherulite aggregate of quartz; (c,d) djurleite (Dju) and barite (Brt) micro veins were present in the quartz or quartz-chlorite (Chl) aggregate.

Figure 14 shows the absolute concentrations of the elements Si, O, Cu, and S along the scanning line of an agate fragment containing native copper in the center of ovoids, which is replaced by growing copper sulphide dendrites. The composition of copper sulphides varies from $\text{Cu}_{1.94}\text{S}$ to $\text{Cu}_{1.75}\text{S}$ and $\text{Cu}_{1.1}\text{S}$, which corresponds to the stoichiometry of such minerals as djurleite, anilite and yarrowite [39].

Table 1 shows the EPMA results of the Cu-S minerals in agates No. 4, 5, 7. The amount of copper and sulphur in sulphides varies, which corresponds to chalcocite (Cu_2S), djurleite ($\text{Cu}_{1.96}\text{S}$), digenite ($\text{Cu}_{1.75-1.78}\text{S}$), anilite ($\text{Cu}_{1.75}\text{S}$), and yarrowite ($\text{Cu}_{1.1}\text{S}$) [39].

Table 1. Representative composition of Cu-S minerals (EPMA data in wt.% and formula) in agates from the Avacha Bay (Eastern Kamchatka, Russia).

No	O	Si	S	Fe	Cu	Total	Formula	Mineral
5/1-1	1.01	-	31.35	0.19	67.48	100.03	$\text{Cu}_{1.1}\text{S}$	yarrowite
5/1-2	1.19	0.43	31.48	-	66.19	99.3	$\text{Cu}_{1.1}\text{S}$	yarrowite
5/1-3	2.28	0.29	21.68	0.26	74.03	98.54	$\text{Cu}_{1.73}\text{S}$	anilite
5/1-4	1.92	0.36	21.99	0.38	75.07	99.72	$\text{Cu}_{1.73}\text{S}$	anilite
5/3-1	1.5	0.49	29.93	0.59	66.32	98.83	$\text{Cu}_{1.12}\text{S}$	yarrowite
5/3-1	3.21		19.98		74.65	97.84	$\text{Cu}_{1.89}\text{S}$	djurleite
5/3-2	2.79	0.37	20.18		76.04	99.54	$\text{Cu}_{1.90}\text{S}$	djurleite
4/1			20.24		79.1	99.34	$\text{Cu}_{1.98}\text{S}$	chalcocite-djurleite
4/26			20.43		78.62	99.05	$\text{Cu}_{1.94}\text{S}$	djurleite
4/27			20.24		78.06	98.30	$\text{Cu}_{1.95}\text{S}$	djurleite
7/2-1	2.11	0.28	20.5		76.17	99.05	$\text{Cu}_{1.88}\text{S}$	djurleite-digenite
7/2-2	2.72	0.64	20.7		74.83	98.89	$\text{Cu}_{1.83}\text{S}$	digenite
7/2-3	1.18	0.28	22.18		75.09	98.73	$\text{Cu}_{1.71}\text{S}$	anilite

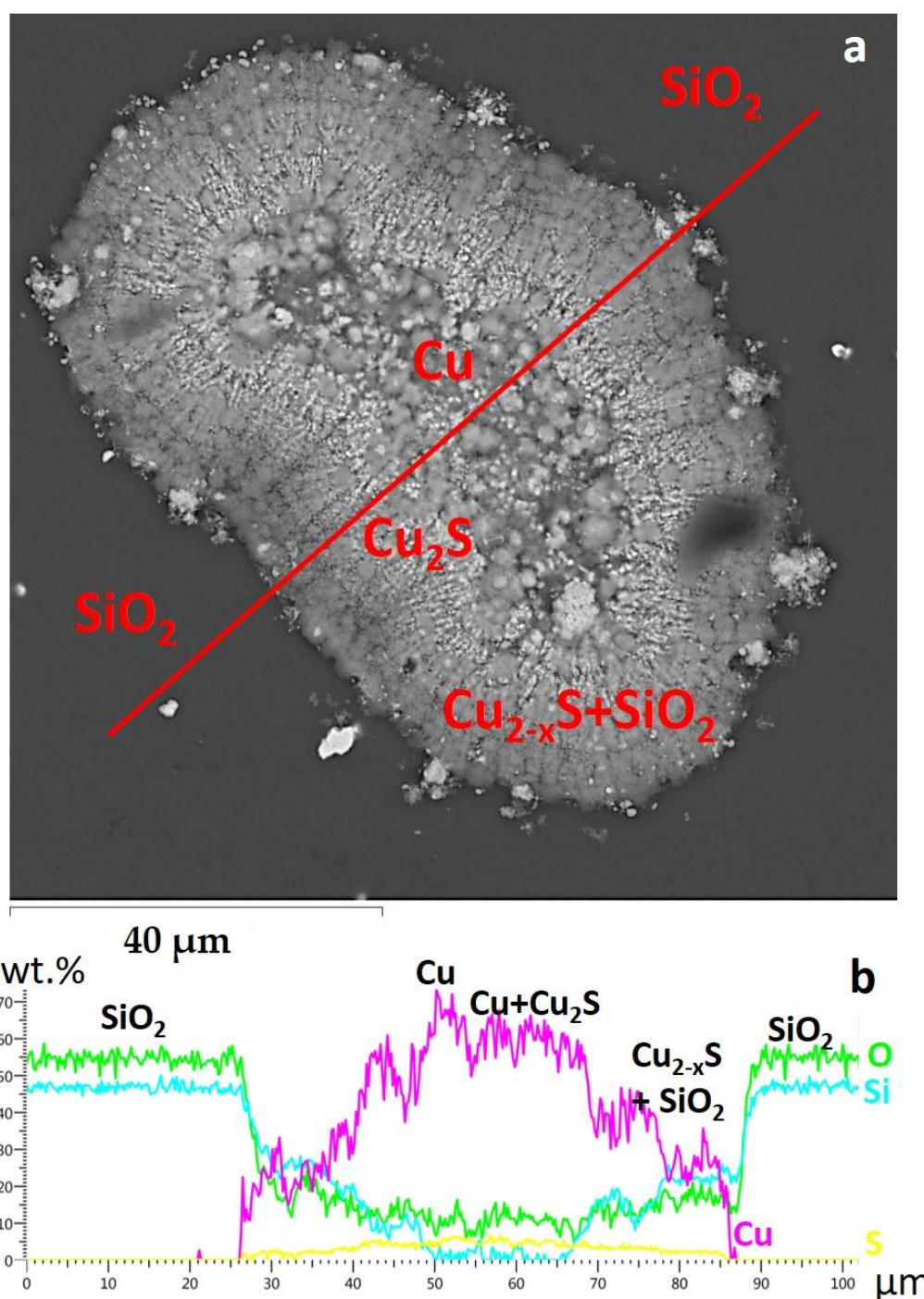


Figure 14. Native copper and dendrites of copper sulphides are present in quartz ovoid (a). Concentrations of the elements Si, O, Cu, and S (b) (in wt.%) are shown along the scanning line of the fragment agate No. 7 (Figure 4f). (a) SEM micrograph.

In the marginal part of agate No. 7 (Figure 4c,f) calcite intergrown with quartz is shown on Figure 15. It contains quartz inclusions and djurleite microinclusions. Some djurleite microinclusions are located at the contact between quartz and calcite or in calcite. Calcite contains Mn impurities up to 0.5 wt.%. The dark zone of quartz around calcite and quartz inclusions in calcite contain Al impurities (0.2–0.3 wt.%).

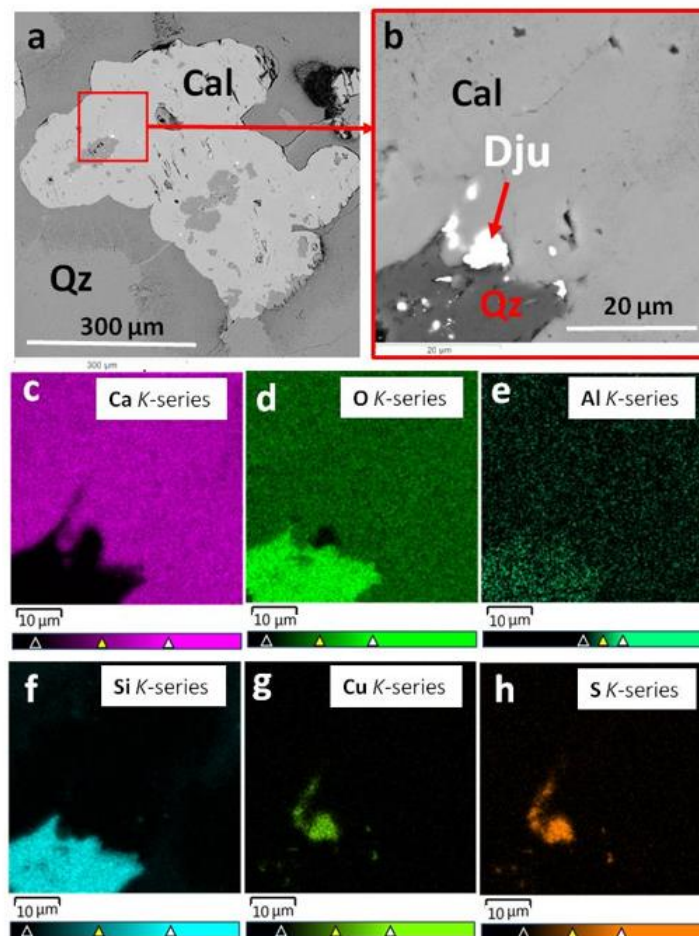


Figure 15. Calcite containing SiO_2 inclusions and djurleite (Dju) micro inclusions in a quartz matrix (a,b) from agate No 7 (Figure 4c,f). Element distribution in a fragment of calcite (Cal) (red square on a) (b) was determined using characteristic rays (c–h). (a,b) SE micrographs.

Microinclusions of djurleite, phlogopite, and K-feldspar are located in quartz matrix (Figure 16a) at the edge of agate No. 4 (Figure 4b,e). Figure 16b–i shows the distribution of Si, O, K, Al, S, Cu, Mg, and Fe over the scanned area.

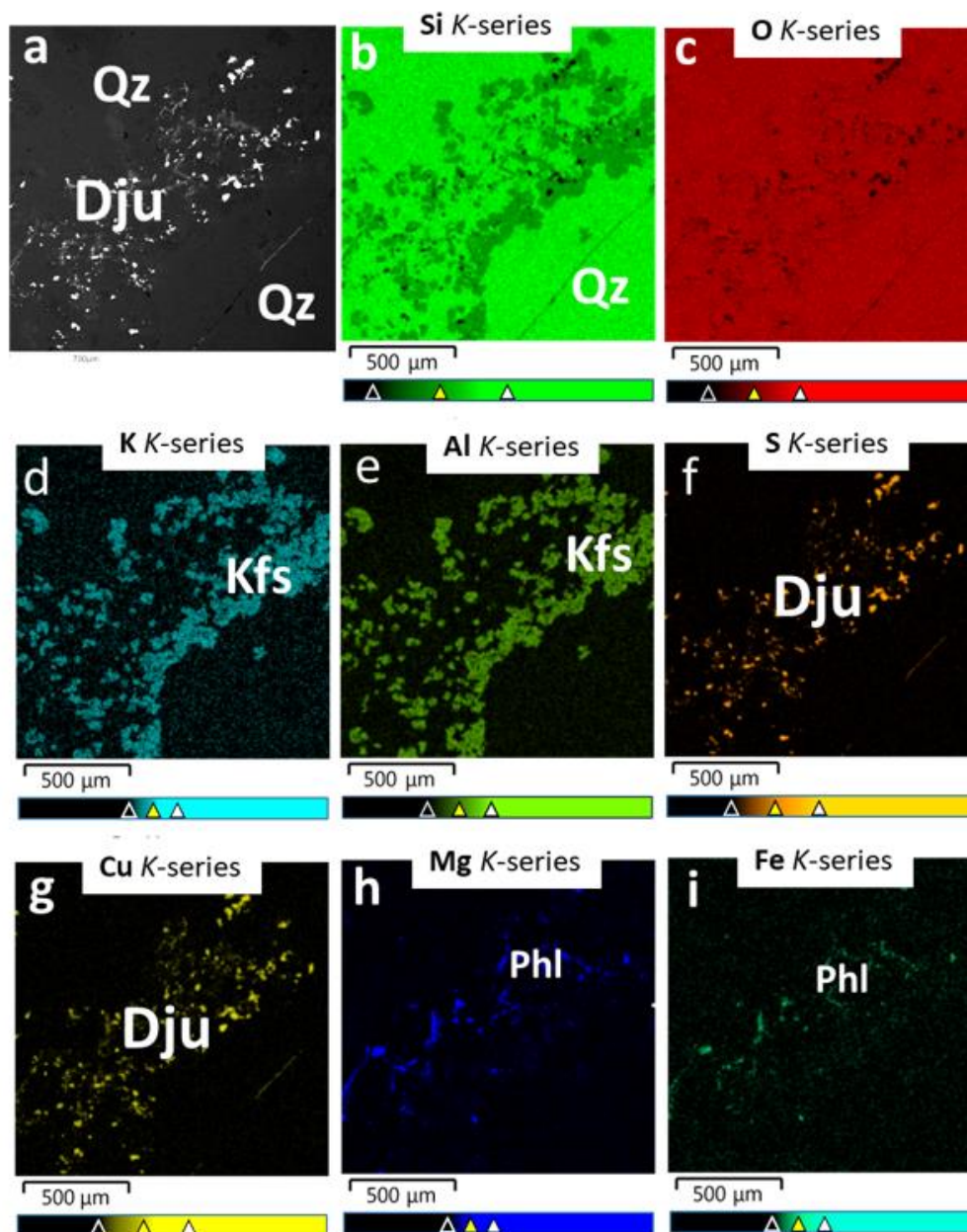


Figure 16. SE micrograph (a) at the edge of agate No 4 (Figure 4b,e) containing micro inclusions of djurleite (Dju), K-feldspar (Kfs), and phlogopite (Phl) in quartz, and maps showing the distribution of the elements over the scanned area (b–i).

In silica interlayers, impurities of elements such as Na, K, Ca, Mg, Al, and Fe are often noted. The concentrations of Fe and Mg vary from 0.2 to 10 wt.%, Na up to 8.7 wt.%, K and Ca up to 4 wt.%, Al up to 7 wt.%. There are sometimes also impurities Cl (up to 2 wt.%), P (up to 0.2 wt.%), Ba (up to 1.4 wt.%), Ti (up to 3 wt.%), Sr (up to 3 wt.%), Mn (up to 0.4 wt.%), V (up to 0.9 wt.%), Cu (up to 3 wt.%), and S (up to 2.6 wt.%). The presence of these impurities is most likely to be associated with the minerals of ore-hosting rocks.

4.4. Results of The Fluid Inclusions Study

Fluid inclusions were found in agate with macrocrystalline quartz in the central part under the faces of individual quartz crystals (Figure 8a). The inclusions trace fragments of crystal growth zones (Figure 17a) and are primary or pseudo-secondary according to the Roedder's classification [36]. In terms

of phase filling, the inclusions are divided into gas single-phase, liquid single-phase, and two-phase, containing a gas bubble and a liquid (Figure 17b–d). In quantitative terms, gas and liquid single-phase inclusions predominate. Two-phase inclusions are rare.

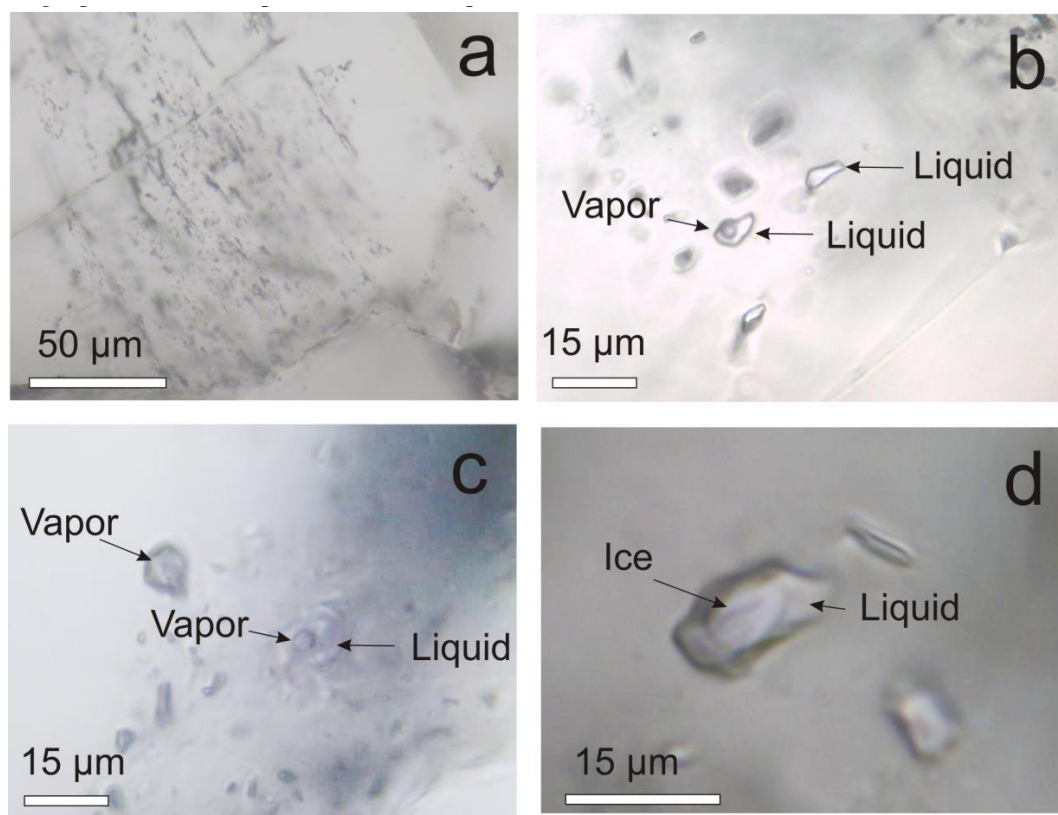


Figure 17. Fluid inclusions in crystalline quartz: (a) a fragment of the growth zone traced by fluid inclusions, (b) two-phase and single-phase water-salt inclusions, (c) single-phase gas and two-phase water-salt inclusions, (d) single-phase water-salt inclusions at a temperature of $-10\text{ }^{\circ}\text{C}$, the frozen-out phase of ice is visible, which finally melts at $-0.3\text{ }^{\circ}\text{C}$.

No liquefaction or freezing of gas was observed with the deep cooling of gas inclusions to a temperature of $-190\text{ }^{\circ}\text{C}$, which demonstrates that its density is low. Phases of eutectic and ice appeared in single-phase and two-phase water-salt inclusions with deep cooling. Melting of the eutectic (the beginning of a noticeable melting of the ice phase) was observed in the temperature range of -55 to $-52\text{ }^{\circ}\text{C}$. The ice phase finally disappeared at a temperature of $-0.3\text{ }^{\circ}\text{C}$. According to the melting point of the eutectic, the composition of solutions of inclusions can be attributed to the water-salt system $\text{CaCl}_2\text{-NaCl-H}_2\text{O}$, with a probable admixture of MgCl_2 [35]. After several cycles of cooling/heating in the temperature range from $+30$ to $-120\text{ }^{\circ}\text{C}$, a small gas bubble appeared in some single-phase water-salt inclusions, which dissolved in the liquid in the range from 110 to $78\text{ }^{\circ}\text{C}$ and lower. The salts concentrations in solution are very low (less than $0.3\text{ wt.}\%$ NaCl eqv.).

Gas-filled two-phase inclusions with a large bubble are homogenized at high temperatures of $250\text{ }^{\circ}\text{C}$ and more, but such temperatures are unrealistic, since sulphide mineralization is confined to amorphous SiO_2 modifications.

The presence of primary gas and two-phase and single-phase liquid fluid inclusions in macrocrystalline quartz indicates boiling of the mineral-forming fluids [36,41,42]. Investigation of the homogenization temperature of two-phase fluid inclusions shows that this quartz could have been formed at temperatures from 110 to $78\text{ }^{\circ}\text{C}$. At the same time, it should be taken into account that agate specimens have undergone many natural freeze-thaw cycles, at least during the Quaternary period. According to Hardie et al. [43], the force of ice crystallization during the cooling of

single-phase inclusions leads to an increase in their volume as a result of ice pressure on the vacuole walls, and then to the appearance of a gas bubble during thawing. It is also possible to assume complete or partial decrepitation of single-phase liquid fluid inclusions during the many cycles of natural freezing-thawing and transformation of single-phase inclusions into two-phase ones. Thus, some of the detected gas and two-phase fluid inclusions in crystalline quartz could be decrepitated, and the measurements of the temperature of homogenization of fluid inclusions could be overestimated relative to the true temperature of their capture. In this case, given the presence of primary single-phase liquid inclusions in crystalline quartz, its crystallization could occur from a homogeneous solution at a temperature lower than 50 °C. Taking into account all the data, the crystallization temperature at the final stages of agate formation could be 110 to 50 °C and lower.

4.5. XRD Results

The content of individual minerals (in wt.%) in the tested samples (No. 4, 5, 7) is automatically calculated by the diffractometer. For example, the X-ray pattern of sample No. 4 is shown in Figure 18. The main phase of the analyzed samples is α -quartz (content 80–90 wt.%). The presence of moganite and cristobalite was also identified. The most intense peaks of these minerals occur in the range of the angles 19–28° 2 θ (Figure 19). Cristobalite is reliably diagnosed by a broad diffraction peak at 21.8° 2 θ [39]. (<https://rruff.info/cristobalite/R060648>). Its content (1–3 wt.%) was determined using the program MATCH and the PDF-4 database based on the calculated intensities of the phases present. The position of the cristobalite peak suggests that this is its low-temperature tetragonal modification. As for moganite, quartz peaks overlap its most intense reflections. Its presence can be judged only by the small shoulders at the base of the quartz reflections. Obviously, the assessment of the content of moganite in the studied samples (6–17 wt.%) has a large error.

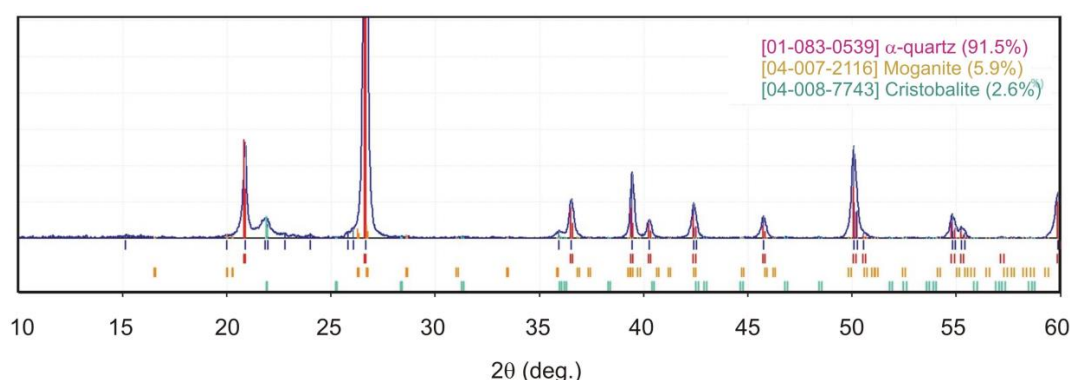


Figure 18. X-ray diffraction pattern of the studied sample (agate No. 4) (CuK α radiation).

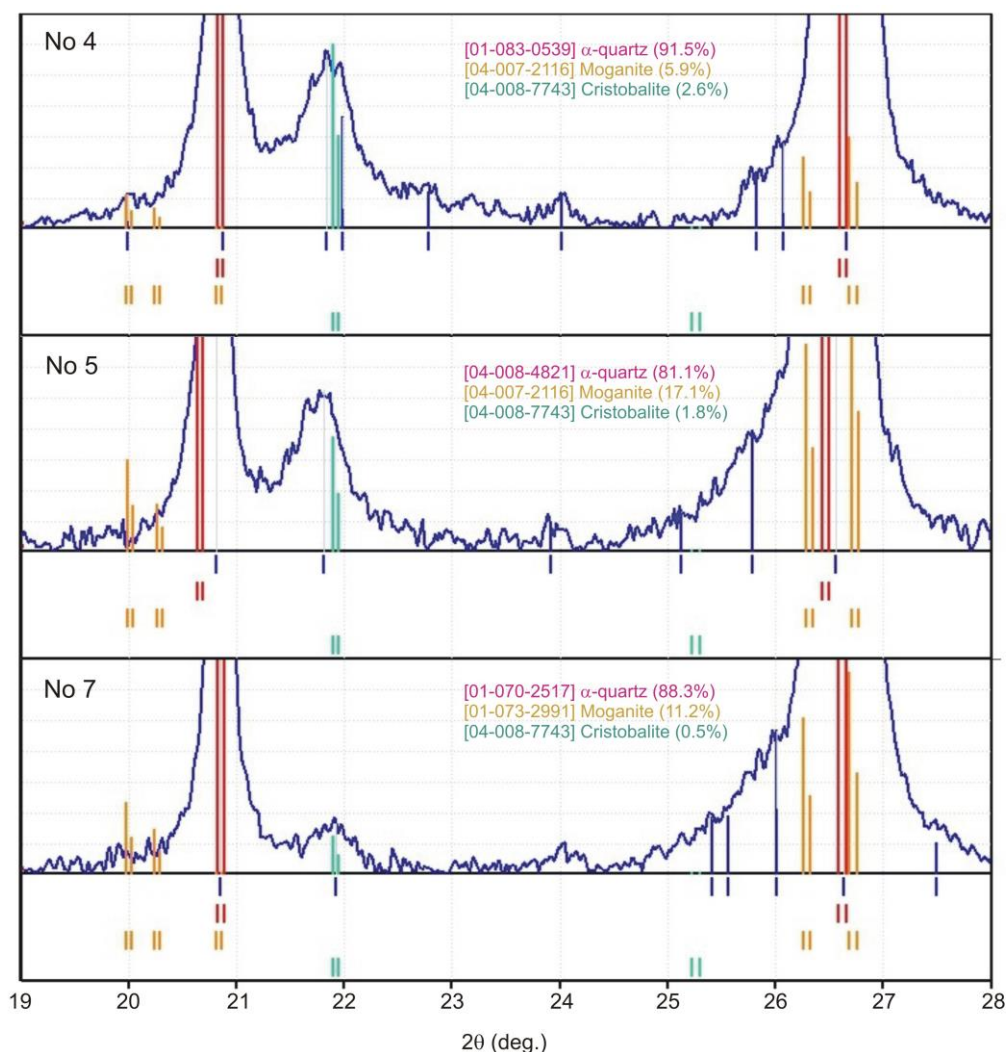


Figure 19. Fragments of X-ray diffraction patterns of the studied samples No. 4, 5, 7, in the range of angles $19\text{--}28^\circ$ 2θ ($\text{CuK}\alpha$ radiation) with the most intense peaks of cristobalite and moganite.

5. Discussion

Agates often contain considerable amounts of mineral inclusions. The mineralogical complexity of agate is a result of its complex formation history [8]. Raman spectroscopy, obtained in the present study, showed that the Avacha Bay agates contained cristobalite in addition to quartz and moganite. XRD results demonstrated that the silica matrix in the agates consists of predominantly α -quartz, low moganite (from 6 to 17 vol.%), and minor cristobalite (1–3 vol.%). The moganite content in agates usually range from 0 to 20% [44,45]. Our data are within this specified interval. This silica polymorph is nearly absent in agates found within relatively old volcanos, but could still be present in relatively young host basaltoids. The preliminary rough estimate of agate age on the examination of moganite content in samples 4, 5, 7 shows a wide variation, from 18 to 48 Ma.

In addition to the silica polymorphs, the native copper, copper sulphides (chalcocite, djurleite, digenite, anilite, yarrowite and chalcopyrite), sphalerite, native silver, barite and cuprite have been identified in the Avacha Bay agates. Native copper occurs as cubic crystals or dendrites in a silica matrix (Figure 5a–c, Figures 8b and 12). Sulphides often cement the marginal parts of spherule aggregates of silica and fill the microveins, which occupy a cross-cutting position with respect to the concentric bands of quartz (Figure 13b–d). Cuprite occurs in intergrowth with native copper and forms microveins in quartz (Figure 8c). The textural relationship between silica and ore minerals suggests that the deposition of native copper occurred simultaneously with the early stage of agate formation.

The deposition of sulphides (copper sulphides and sphalerite), barite and cuprite occurred later and is apparently associated with the second stage of agate formation.

In the agates of the Avacha Bay, copper mineralization is characterized as a two-stage character. The idiomorphic crystals of native copper and clear boundaries with the silica matrix makes it possible to make judgments about the possible simultaneous crystallization. Native copper in the absence of copper sulphides and cuprite indicates a slight deficiency of sulfur and reducing conditions in an early stage. The replacement of native copper with copper sulphides in the pore and interstitial space of spheroidal-layered silica aggregates occurs with the participation of later solutions containing $H_2S(aq)$ or Cu-ions, which leads to the sulphurisation of native copper and later the deposition of Cu-S minerals. The presence of barite and copper sulphides filling the cracks indicates redox conditions close to sulfide-sulfate $H_2S/H_2SO_4^-$ equilibrium [46]. The presence of cuprite indicates their later deposition and the oxidizing conditions. Cuprite and copper sulphides are a typical secondary mineral, which accompanies native copper in the oxidized zone of copper sulphide deposits [47].

According to the Cu-S phase diagram [46], djurleite is stable at <93 °C and anilite <75 °C. Our results of the fluid inclusions study show that the crystallization temperature at the final stages of agate formation could be 110 to 50 °C and below. The absence of fluid inclusions in the entire volume of agate nodules does not allow one to estimate the entire temperature range of the formation of the studied agates. The minimum homogenization temperatures for agates from volcanic rocks of some German occurrences vary between 95 and 186 °C [8]. Analogic data for deposits in the north-east of Russia show 120–170 °C [4]. The P,T-parameters of the zeolite facies are spread in the sequence of volcanic rocks, containing agates: 90–290 °C, 1–5 kb [12]. There is a general consensus that agates in basic igneous hosts form at <100 °C [48].

According to Götze et al. [8], in agates from basic and intermediate rocks, quartz mostly contains inclusions having low salinity (<4 wt.% NaCl eqv.). The results obtained in this study are in good agreement with these data. The concentrations of salts in the composition of fluid inclusions in agates from Avacha Bay are a very low (less than 0.3 wt.% NaCl eqv.). The main salt components were $CaCl_2$ and NaCl with a probable admixture of $MgCl_2$.

The presence of calcite in the intergrowth with quartz in the marginal parts of some agates (No. 7), containing microinclusions of djurleite at the contact of quartz (Figure 15), indicates the participation of Ca^{2+} -, CO_3^{2-} -ions in low hydrothermal solution at early stage. Geochemical investigations of calcite in agates provide a temperature of crystallization in the range between 20 and 230 °C [7,49].

The relationships between native copper, copper sulphides and quartz in the Avacha Bay agates differ from other locations—the Ayaguz agate deposit (East Kazakhstan) [18], the Wolverine Mine, Wolverine, Houghton County, Michigan (USA) [19,21], Rudno near Krzeszowice in Lower Silesia (Poland) [25], Sidi Rahal, and Kerrouchen (Khénifra Province, Meknés-Tafilalet Region) in the Atlas mountains of Morocco [26,27]. For example, native copper found in agates from Rudno near Krzeszowice in Lower Silesia (Poland) [25] suggests its secondary origin. The formation of vein agates within spilitized (albite-rich) alkali-basalts from the upper parts of Borówno quarry (Intra-Sudetic Basin) (Lower Silesia, Poland) was marked by recrystallization of metastable silica phases (i.e., moganite), coupled with the local replacement of pre-existing sulphates and/or carbonates by silica during boiling-related conditions [28].

Rosemeyer [19,21] shows the Kearsarge copper-bearing agate photos confirming a partial or almost complete replacement of the chalcedony banding by native copper. This replacement mechanism does not explain the relationships of quartz with native copper in the agates from Avacha Bay. The replacement mechanism is a more appropriate explanation for the formation of a late-stage copper sulfide with the participation of H_2S solutions (Figures 13 and 14). The genesis of the native copper lodes on the Keweenaw Peninsula of northern Michigan is most commonly explained by a metamorphogenic model [50]. A meteoric and metamorphic model was also developed by Brown [51,52].

The identification of copper in the Avacha Bay agates suggests a potential copper source in the surrounding basalts. According to our RFA analysis data, the amount of copper in them is 160 ppm,

which is more than Clarke content, containing 55 ppm [53]. More than 30 areas of basaltic lavas worldwide are known for containing native copper, some of which occur in deposits of potential commercial importance [47]. In 15 of these areas, certain flows contain moderate amounts of finely disseminated primary native copper, whereas the remaining flows contain little or no visible copper. The native copper dendrites in rock fragments in coastal outcrops of the Avacha Bay were found by E.Sidorov, one of the authors of the first paper on agates with native copper in Kamchatka [29]. The photo of this sample is shown on Figure 3. The low-temperature waters could be responsible for the transport of copper. The source of fluid is a task for future research.

It should be noted that agates containing native copper were found in areas where large deposits of native copper are known; Turin mines (Ural) [54], Dzhezkazgan (Kazakhstan) [18], and Michigan (Keweenaw Peninsula, USA) [19,21,50–52]. Preliminary data were obtained on the presence of native silver in some agates from Avacha Bay. The presence of Cu, Ag, Zn, Sr, and V-bearing ore occurrences is predicted.

6. Conclusions

- (1) Copper mineralization in agates from the Avacha Bay (Eastern Kamchatka, Russia) is represented by native copper, as well as copper sulphides (chalcocite, djurleite, digenite, anilite, yarrowite, rarely chalcopyrite) and cuprite. In addition to copper minerals, sphalerite and native silver are also found in agates from this location.
- (2) Raman spectroscopy and XRD results demonstrated that the Avacha Bay agates contained cristobalite in addition to quartz and moganite. The substance of “moss” formations is represented by an aggregate of cristobalite and fluorophlogopite $\text{KMg}_3(\text{Si}_3\text{Al})\text{O}_{10}\text{F}_2$.
- (3) The native copper crystallized simultaneously with early silica. Copper sulphides, sphalerite, native silver, cuprite, and barite were deposited later apparently with the participation of low temperature hydrotherms with H_2S , which were replaced by sulphate solutions caused by a change in redox change in hypergenic conditions.
- (4) Macrocrystalline quartz in the center of agate nodules could be formed at a temperature from 110 to 50°C and below. The main salt components of the fluid inclusions in macrocrystalline quartz were CaCl_2 and NaCl with a probable admixture of MgCl_2 . The salt concentration of solutions is lower than 0.3 wt.% NaCl equivalent.
- (5) The surrounding basalts could be the source of copper for agates of the Avacha Bay. The presence of copper minerals and other ore elements in agates of volcanogenic strata of Eastern Kamchatka can serve as a direct indicator of the high ore potential in this territory.

Author Contributions: Conceptualization, methodology, G.P. and E.S.; investigation, A.B. and Y.S.; writing and editing, G.P.; visualization G.P., E.S., A.B. and Y.S.; supervision G.P. All authors have read and agreed to the published version of the manuscript.

Funding: The studies were carried out within the framework of the state assignment of the Sobolev Institute of Geology and Mineralogy of Siberian Branch of Russian Academy of Sciences and by the grant no. 13.1902.21.0018 “Fundamental Problems of the Development of the Mineral Resource Base of the High-Tech Industry and Energy in Russia” from Ministry of Science and Higher Education of the Russian Federation.

Acknowledgments: The authors thank N. Karmanov, M. Khlestov (VS Sobolev Institute of Geology and Mineralogy, Siberian Branch, Russian Academy of Sciences) and V. Chubarov (Institute of Volcanology and Seismology, Far East Branch of Russian Academy of Sciences) for help in carrying out a large amount of work on a scanning electron microscope and an X-ray spectral microanalyzer. We are grateful to A. Vishnevskii for macrophotographs of agates (Figure 4) and D. Bukhanova for photograph of agate amygdales in basalt (Figure 2b). The authors also thanks V. Zinina and T. Zhuravkova. We would like to thank T. Moxon (visiting research worker, Cambridge University) for the invaluable advices. We are very grateful to Lucyna Natkaniec-Nowak (AGH University of Science and Technology, Kraków, Poland) and three anonymous reviewers for their comments, which helped to improve the quality of the paper. Appreciation is given to the Academic Editor for careful reading of the manuscript and comments.

Conflicts of Interest: The authors declare no conflict of interest.

References

1. Tripp, R.B. The mineralogy of Warsaw Formation geodes. *Iowa Acad. Sci. Proc.* **1959**, *66*, 350–356.
2. Barsanov, G.P.; Yakovleva, M.E. Mineralogy, macro- and micromorphological features of agates. *New Data Miner.* **1982**, *30*, 3–26. (In Russian)
3. Godovikov, A.A.; Ripinen, O.I.; Motorin, S.G. *Agates*; Nedra: Moscow, Russia, 1987; p. 368. (In Russian)
4. Goncharov, V.I.; Gorodinsky, M.E.; Pavlov, G.F.; Savva, N.E.; Fadeev, A.P.; Vartanov, V.V.; Gunchenko, E.V. *Chalcedony of North-East of the USSR*; Science: Moscow, Russia, 1987; p. 192. (In Russian)
5. Heaney, P.J. A proposed mechanism for the growth of chalcedony. *Am. Min.* **1993**, *115*, 66–74. [[CrossRef](#)]
6. Graetsch, H. Structural characteristics of opaline and microcrystalline silica minerals. In *Silica. Rev. Mineral.* **1994**, *29*, 209–232.
7. Götze, J.; Tichomirow, M.; Fuchs, H.; Pilot, J.; Sharp, Z.D. Chemistry of agates: A trace element and stable isotope study. *Chem. Geol.* **2001**, *181*, 523–541. [[CrossRef](#)]
8. Götze, J.; Möckel, R.; Pan, Y. Mineralogy, geochemistry and genesis of agate—A review. *Minerals* **2020**, *10*, 1037. [[CrossRef](#)]
9. Moxon, T.; Ríos, S. Moganite and water content as a function of age in agate: An XRD and thermogravimetric study. *Eur. J. Mineral* **2004**, *16*, 269–278. [[CrossRef](#)]
10. Moxon, T. *Studies on Agate: Microscopy, Spectroscopy, Growth, High Temperature and Possible Origin*; Terra Publications: Doncaster, UK, 2009; p. 96.
11. Lyashenko, E.A. Agates of Russia. *Mineral. Alm.* **2010**, *15*, 6–27. (In Russian)
12. Spiridonov, E.M.; Ladygin, V.M.; Yanakieva, D.Y.; Frolova, J.V.; Semikolennykh, E.S. Agates in metavolcanics. Bulletin of the Russian Federal Property Fund. 2014. Available online: https://www.rfbr.ru/rffi/ru/bulletin/o_1923809#8 (accessed on 22 October 2020).
13. Ottens, B.; Götze, J.; Schuster, R.; Krenn, K.; Hauzenberger, C.; Zsolt, B.; Vennemann, T. Exceptional multi-stage mineralization of secondary minerals in cavities of flood basalts from the Deccan Volcanic Province, India. *Minerals* **2019**, *1019*, 351. [[CrossRef](#)]
14. Gliozzo, E. Variations on the silica theme: Classification and provenance from Pliny to current supplies. *EMU Notes Mineral.* **2019**, *2*, 13–85.
15. Pršek, J.; Dumańska-Słowik, M.; Powolny, T.; Natkaniec-Nowak, L.; Tobiła, T.; Zych, D.; Skrepnicka, D. Agates from Western Atlas (Morocco)—Constraints from mineralogical and microtextural characteristics. *Minerals* **2020**, *10*, 198. [[CrossRef](#)]
16. Moxon, T. A re-examination of water in agate and its bearing on the agate genesis enigma. *Min. Mag.* **2017**, *81*, 1223–1244. [[CrossRef](#)]
17. Zhang, X.; Ji, L.; He, X. Gemological characteristics and origin of the Zhanguohong agate from Beipiao, Liaoning province, China: A combined microscopic, X-ray diffraction, and Raman spectroscopic study. *Minerals* **2020**, *10*, 401. [[CrossRef](#)]
18. Yusupov, S.S. Thermobarogeochemical Conditions for the Formation of Agate Deposits in the Urals and Kazakhstan. In *Questions of Mineralogy, Geochemistry and Genesis of Minerals of the Southern Urals*; Bashk. Prince Publishing House: Ufa, Russia, 1982; pp. 92–99.
19. Rosemeyer, T. The Kearsarge copper-bearing amygdaloidal lode, Houghton and Keweenaw countries, Michigan. *Rocks Miner.* **2007**, *82*, 276–297. [[CrossRef](#)]
20. Rosemeyer, T. A spectacular find of amygdaloidal agates with native copper inclusions from Michigan's Copper Country. *Rocks Miner.* **2001**, *76*, 403. [[CrossRef](#)]
21. Rosemeyer, T. Copper-banded Agates from the Kearsarge Copper-bearing Amygdaloidal Lode, Houghton County, Michigan. *Rocks Miner.* **2012**, *87*, 352–365. [[CrossRef](#)]
22. Radko, V.A. *Agates, Carnelian, Jasperoids of Norilsk*; GeoKniga: St. Petersburg, Russia, 2013; p. 128.
23. Dumańska-Słowik, M.; Natkaniec-Nowak, L.; Kotarba, M.J.; Sikorska, M.; Rzymelka, J.A.; Łoboda, A.; Gaweł, A. Mineralogical and geochemical characterization of the “bituminous” agates from Nowy Kościół Lower Silesia. *N. Jb. Miner. Mh.* **2008**, *184*, 255–268. [[CrossRef](#)]
24. Nezafati, N.; Momenzadeh, M.; Pernicka, E. Darhand Copper Occurrence: An Example of Michigan-Type Native Copper Deposits in Central Iran. In *Mineral Deposit Research: Meeting the Global Challenge*; Mao, J., Bierlein, F.P., Eds.; Springer: Berlin/Heidelberg, Germany; New York, NY, USA, 2005; Volume 1, pp. 165–166.
25. Krawczyński, W. Native copper in agates from Rudno near Krzeszowice. *Mineral. Pol.* **1995**, *26*, 27–32.

26. Dumańska-Słowik, M.; Natkaniec-Nowak, L.; Weselucha-Birczyńska, A.; Gawel, A.; Lankosz, M.; Wróbel, P. Agates from Sidi Rahal, in the Atlas Mountains of Morocco: Gemmological characteristics and proposed origin. *Gems Gemol.* **2013**, *49*, 148–159. [[CrossRef](#)]
27. Natkaniec-Nowak, L.; Dumańska-Słowik, M.; Pršek, J.; Lankosz, M.; Wróbel, P.; Gawel, A.; Kowalczyk, J.; Kocemba, J. Agates from Kerrouchen (the Atlas Mountains, Morocco): Textural types and their gemological characteristics. *Minerals* **2016**, *6*, 77. [[CrossRef](#)]
28. Powolny, T.; Dumańska-Słowik, M.; Sikorska-Jaworowska, M.; Wójcik-Bania, M. Agate mineralization in spilitized Permian volcanics from “Borówno” quarry (Lower Silesia, Poland)—Microtextural, mineralogical, and geochemical constraints. *Ore Geol. Rev.* **2019**, *114*, 103–130. [[CrossRef](#)]
29. Sidorov, E.G.; Kutjev, F.T.; Anikin, P.P. Native Copper Agates of the Kuril-Kamchatka Province. In *Native Metals in Postmagmatic Formations*; Yakutsk Publishing House: Yakutsk, Russia, 1985; pp. 72–73. (In Russian)
30. Sheymovich, V.S. *The State Geological Map of the Russian Federation, Scale 1:200,000*; South-Kamchatka Series. Sheets N_57_XXI (Northern Koryaks), N_57_XXVII (Petropavlovsk-Kamchatsky), N_57_XXXIII (Mutnovskaya hill); Explanatory Note: Moscow, Russia, 2000; p. 302. (In Russian)
31. Savelyev, D.P.; Palechek, T.N.; Portnyagin, M.V. Campanian oceanic siliceous-volcanogenic deposits in the basement of the Eastern Kamchatka volcanic belt. *Pac. Geol.* **2005**, *24*, 46–54. (In Russian)
32. Frolova, Y.V.; Blyumkina, M.E.; Bolshakov, I.E.; Ermolinsky, A.B. *Comparative Petrophysical Characteristics of Volcanic Rocks of the Cretaceous and Miocene Age of Avacha Bay. Volcanism and Related Processes*; Materials of the XXIII Annual Scientific Conference Dedicated to the Volcanologist’s Day; IViS: Petropavlovsk-Kamchatsky, Russia, 2020; pp. 68–71.
33. Saveliev, D.P. A scattering of agates at Cape Vertikalny, Eastern Kamchatka. *Bull. Kamchatka Reg. Assoc. Educ. Sci. Cent. Ser. Earth Sci.* **2020**, *47*, 3. [[CrossRef](#)]
34. *The Powder Diffraction File PDF-4p*; International Centre for Diffraction Data: Newtown Square, PA, USA, 2009.
35. Borisenko, A.S. Analysis of the Salt Composition of solutions of gas-liquid inclusions in minerals by cryometry. In *The Use of Methods of Thermobarogeochemistry in the Search and Study of Ore Deposits*; Laverova, N.P., Ed.; Nedra: Moscow, Russia, 1982; pp. 37–47. (In Russian)
36. Roedder, E. Fluid inclusions. *Rev. Mineral.* **1984**, *12*, 79–108.
37. Bodnar, R.J.; Vityk, M.O. Interpretation of microthermometric data for NaCl–H₂O fluid inclusions. In *Fluid Inclusions in Minerals: Methods and Applications*; De Vivo, B., Frezzotti, M.L., Eds.; Virginia Polytechnic Inst State Univ: Blacksburg, VA, USA, 1994; pp. 117–131.
38. Dong, G.; Morrison, G.; Jaireth, S. Quartz textures in epithermal veins, Queensland; classification, origin, and implication. *Econ. Geol.* **1995**, *90*, 1841–1856. [[CrossRef](#)]
39. Lafuente, B.; Downs, R.T.; Yang, H.; Stone, N. The power of databases: The RRUFF project. In *Highlights in Mineralogical Crystallography*; Armbruster, T., Danisi, R.M., Eds.; W. De Gruyter: Berlin, Germany, 2015; pp. 1–30.
40. Götze, J.; Nasdala, L.; Kleeberg, R.; Wenzel, M. Occurrence and distribution of “moganite” in agate/chalcedony: A combined micro-Raman, Rietveld, and cathodoluminescence study. *Contrib. Mineral. Petrol.* **1998**, *133*, 96–105. [[CrossRef](#)]
41. Bodnar, R.J. Interpretation of data from aqueous-electrolyte fluid inclusions. In *Fluid Inclusions: Analysis and Interpretation*; Samson, I., Anderson, A., Marshall, D., Eds.; Short Course Series; Mineralogical Association of Canada: Ottawa, ON, Canada, 2003; pp. 81–100.
42. Goldstein, R.H.; Reynolds, T.J. *Systematics of Fluid Inclusions in Diagenetic Minerals*; SEPM Short Course: Tulsa, OK, USA, 1994; Volume 31, p. 199.
43. Hardie, L.A. Origin of CaCl₂ brines by basalt-seawater interactions insights provided by some simple mass balance calculations. *Contrib. Mineral. Petrol.* **1983**, *82*, 205–213. [[CrossRef](#)]
44. Heaney, P.J.; Post, J.E. The Widespread Distribution of a Noel Silica Polymorph in Microcrystalline Quartz Varieties. *Science* **1992**, *255*, 441–443. [[CrossRef](#)]
45. Moxon, T.; Carpenter, M.A. Crystallite growth kinetics in nanocrystalline quartz (agate and chalcedony). *Miner. Mag.* **2009**, *73*, 551–568. [[CrossRef](#)]
46. Barton, P.B., Jr.; Skinner, R.J. Sulphide mineral stabilities. In *Geochemistry of Hydrothermal Ore Deposits*; Barnes, H.L., Ed.; Wiley: New York, NY, USA, 1979; pp. 278–403.
47. Cornwall, H.R. A summary of ideas on the origin of native copper deposits. *Econ. Geol.* **1956**, *51*, 615–631. [[CrossRef](#)]

48. Moxon, T.; Palyanova, G. Agate genesis: A continuing enigma. *Minerals* **2020**, *10*, 953. [[CrossRef](#)]
49. Gilg, H.A.; Morteani, G.; Kostitsyn, Y.; Preinfalk, C.; Gatter, I.; Strieder, A.J. Genesis of amethyst geodes in basaltic rocks of the Serra Geral Formation (Ametista do Sul, Rio Grande do Sul, Brazil): A fluid inclusion, REE, oxygen, carbon, and Sr isotope study on basalt, quartz, and calcite. *Miner. Depos.* **2003**, *38*, 1009–1025. [[CrossRef](#)]
50. Stoiber, R.E.; Davison, E.S. Amygdule mineral zoning in the Portage Lake lava series, Michigan copper district. *Econ. Geol.* **1959**, *54*, 1444–1460. [[CrossRef](#)]
51. Bornhorst, T.J. Tectonic context of native copper deposits of the North American Midcontinent rift system. *Geol. Soc. Am. Spec. Pap.* **1997**, *312*, 127–136.
52. Brown, A.C. Genesis of native copper lodes in the Keweenaw district, northern Michigan: A hybrid evolved meteoric and metamorphic model. *Econ. Geol.* **2006**, *101*, 1437–1444. [[CrossRef](#)]
53. Taylor, S.R. Abundance of chemical elements in the continental crust: A new table. *Geochim. Cosmochim. Acta* **1964**, *28*, 1273–1285. [[CrossRef](#)]
54. Savchuk, Y.S.; Volkov, A.V.; Aristov, V.V. Cupriferous basalts of the Northern Urals. *Litosfera* **2017**, *17*, 133–144.

Publisher’s Note: MDPI stays neutral with regard to jurisdictional claims in published maps and institutional affiliations.



© 2020 by the authors. Licensee MDPI, Basel, Switzerland. This article is an open access article distributed under the terms and conditions of the Creative Commons Attribution (CC BY) license (<http://creativecommons.org/licenses/by/4.0/>).